Research Article | Vol. 26, No. 21 | 15 Oct 2018 | OPTICS EXPRESS 28161
Optics EXPRESS

One-step generation of hybrid micro-optics with high-frequency diffractive structures on infrared materials by ultra-precision side milling

ZHANWEN SUN, SUET TO,* AND K. M. YU

State Key Laboratory in Ultra-Precision Machining Technology, Department of Industrial and Systems Engineering, The Hong Kong Polytechnic University, Kowloon, Hong Kong
**sandy.to@polyu.edu.hk*

Abstract: Hybrid micro-optics of infrared (IR) materials are of great advantage in realizing the function integration and minimization of advanced IR optical systems. However, due to the hard-and-brittle nature of IR materials, it is still challenging for both non-mechanical and mechanical technologies to achieve one-step generation of hybrid infrared micro-optics with high form accuracy. In the present study, a flexible method, namely ultra-precision side milling (UPSM), is first introduced to achieve one-step generation of infrared hybrid micro-optics in ductile mode, and the corresponding reflective diffraction characteristics are analyzed. In UPSM, the reflective/refractive primary surface of the hybrid micro-optics is formed via the removal of workpiece material, and the high-frequent secondary diffractive micro/nanostructures are simultaneously generated by the tool residual marks of cutting trajectories. With the consideration of the changing curvature of the primary surface, the optimal toolpath generation strategy is introduced to acquire the desired shapes of the secondary micro/nanostructures, and the selecting criteria of the machining parameters is discussed to avoid the brittle fractures of IR materials. In practice, two types of hybrid micro-optic components, namely hybrid micro-aspheric arrays and sinusoid grid surface with high-frequent secondary unidirectional phase gratings, are successfully fabricated on single-crystal silicon to validate the proposed method. The method adopted in this study is very promising for the deterministic fabrication of hybrid micro-optics on infrared materials.

1. Introduction

Hybrid micro-optics of infrared (IR) materials has attracted widespread attention for a variety of applications in advanced IR optical systems, due to its unique advantages for function integration and minimization [1–3]. For example, hybrid micro-lens arrays with the imposition of hierarchical nanostructures enable a better antireflective property compared with conventional ones [3]. Hybrid micro-optics constructed by high-frequent secondary nanometric phase gratings generally comprise both reflective/refractive as well as high-frequent diffractive functions, which is helpful for the creation of new optics systems and the improvement of the optics performance [4]. However, most IR materials, such as silicon and germanium, are characterized as hard-and-brittle nature with very low fracture toughness, which imposes great difficulties in the fabrication of infrared optical components with ultra-smooth surfaces and ultra-precision form accuracy for both non-mechanical and mechanical technologies. It is known that once the undeformed chip thickness is beyond a critical value, brittle fractures will vastly generate and severely destroy the finished surfaces of IR materials [5]. This difficult-to-machine nature of IR materials can be more significant in the fabrication of hybrid optics with complicated hierarchical micro/nanostructures. Generally, complex machining technologies that combines multi-step machining processes are required to

#344339 https://doi.org/10.1364/OE.26.028161
Journal © 2018 Received 30 Aug 2018; revised 26 Sep 2018; accepted 26 Sep 2018; published 12 Oct 2018

Optics EXPRESS

generate hybrid structures on IR materials, which is very low-efficient and difficult to control form accuracy [6–8].

Various non-mechanical machining methods based on lithographic technologies, such as electron beam lithography, focused ion bean and laser ablation, have been proposed to fabricate diffractive micro/nanostructures on IR materials [9–11]. Although these methods have been demonstrated to be effective for the construction of micro/nanostructures with very high resolution, they are commonly restricted to planar substrates or simple concave/convex surfaces with a large radius of curvature [9]. To obtain the hybrid IR micro-optics with desired shapes, multi-step processes that combines ultra-precision machining and picosecond laser ablation was normally required [3]. In this case, ultra-precision machining methods are applied to generate the refractive/reflective primary surface, which is further processed using the picosecond laser ablation to construct secondary high-frequent diffractive structures. Nevertheless, this hybrid process not only introduce unnecessary machining errors, but also is relatively high-cost and low-efficient. Similarly, etching methods, dominated by laser-assed and chemical etching, are also applied to construct secondary diffractive micro/nanostructures on the processed primary surfaces to form hybrid IR optical components [12–14]. In practical, these methods normally require very expensive facilities, and are difficult to generate complex secondary structures due to the uncontrolled etching direction. Femtosecond laser polymerization is a promising method to form hybrid structures in a flexible way, but this method highly restricts to low efficiency and photocurable polymer materials. Therefore, to achieve one-step generation of hybrid IR freeform micro-optics with high form accuracy as well as low processing time is still challenging for non-mechanical methods.

Ultra-precision diamond cutting technologies, dominated by fast and slow tool servo (FTS/STS), vibration-assisted cutting and diamond milling, are more promising for the deterministic generation of hybrid IR micro-optics with complex shapes, due to their capability of achieving ultra-smooth surface quality as well as ultra-high from accuracy [15–17]. Slow tool servo system upgrades from the diamond turning by applying the servo motion on the spindle. In the machining process, the spindle and the x slide move with a constant speed, and structured surfaces can be generated with the assistance of the oscillations of the z slide. The configuration of fast tool servo (FTS) is similar to that of slow tool servo, but FTS possesses a much higher frequency movement in z direction normally driven by piezoelectric ceramics or voice-coil motor. By means of FTS/STS, freeform surfaces and some simple micro-structures, such as Fresnel lens and micro-sphere lens arrays, have been successfully fabricated on brittle IR materials with high form quality [18,19]. The advantage of FTS/STS is its flexibility for deterministic generation of microstructures with nanometric surface roughness and sub-micrometric form accuracy [20]. However, because of the bandwidth limitation of the servo system, the resolution of the microstructures fabricated using FTS/STS generally ranges in a few hundred micrometers, which highly restrict the highest attainable periodicity of the secondary diffractive micro/nanostructures of hybrid micro-optics. Besides, to avoid brittle fractures, very small machining parameters, i.e. feed rates and depths of cut, are necessarily adopted in FTS/STS of brittle IR materials, which further limit the achievable height variation of the generated hybrid IR surfaces [21].

With the assistance of the high-frequent vibration, much higher resolution of secondary micro/nanostructures can be achieved by ultrasonic vibration-assisted diamond cutting (UVAC) [22,23]. In UVAC, the diamond tool normally vibrates elliptically with a very high frequency in the plane determined by the chip flow direction and the normal cutting direction [22]. For the hybrid micro-grooves generated by UVAC, the micro-dimples constructed by the tool residual marks between two connective elliptical loci serve as the hierarchical structures. In this case, the material is removed in a way similar to plunge cutting, so brittle fractures will easily generate at a higher depth of cut. Especially, this method is only suitable for planer surface, and is hard for UVAC to generate the hybrid structures with a freeform primary surface.

Optics EXPRESS

Compared with FTS/STS and UVAC, diamond milling is more convenient to generate functional surfaces with uniform surface quality, because of its process consistency and flexible tool path generation. Diamond milling employs a rotational diamond tool to remove the material. The different clamped styles of the diamond tool lead to different definitions of the milling processes. Diamond milling generally can be classified into diamond face milling and fly cutting. Face milling is characterized as a rotational ball milling tool with its axis perpendicular to the workpiece. Even though face milling is flexible in the generation of freeform surface or micro lens arrays, this method cannot be used to fabricated hybrid structures with high-frequent secondary nanostructures, due to the limitation of size of the gyration radius. Besides, the commercial ball milling tools used in face milling may not be able to be designed with a desired negative rake angle, which is easy to cause brittle fractures in the machining of brittle IR materials [16]. According to zhang et al. [24], fly cutting generally relate to the rotational diamond tool with a large swing radius (over 30 mm). It has been demonstrated that the intermittent cutting process of fly cutting is more beneficial to the ductile machining of IR materials [5]. However, the large swing radius of fly cutting will easily lead to the interference between tool path and the finished surface, thereby highly restricting the curvature radius of the primary surface.

For milling, previous toolpath generation strategies designed for continuous freeform surfaces cannot be directly applied in the fabrication of hybrid optics on infrared materials. The unique scenarios in the fabrication of hybrid structures should be considered, and new and special contents in terms of toolpath generation algorithm for hybrid structures need to be optimized. For example, the size and shape of constructed secondary diffractive nanostructures need to be uniform for hybrid micro-optics, regardless of the curvature changes of the reflective/refractive primary surface. Nevertheless, previous strategies generally neglect the uniformity of tool residual marks, which inevitably induces a non-uniform secondary nanostructure for hybrid optics. Besides, in order to acquire the desired hybrid shapes with high form accuracy on infrared materials, the selecting criteria of the machining parameters, including swing radius and feed rate, is also different from that of ordinary ones.

Overall, it is still challenging for both non-mechanical and mechanical technologies to achieve one-step generation of hybrid infrared micro-optics that is characterized as a complex freeform primary surface with the imposition of high-frequent diffractive secondary micro/nanostructures. In this paper, a novel ultra-precision side milling (UPSM) method first adopted for the fabrication of hybrid micro-optics on IR materials in ductile mode. In UPSM, an insert diamond tool tip is adopted instead of a diamond turning tool or ball milling tool. Fang et al. [25] made a definition on milling that if the diamond tool is close to the axis of rotation, this process is commonly referred to as raster milling. Based on this definition, both the face milling and the proposed UPSM are under the definition of raster milling. Nevertheless, in face milling using a ball milling tool, the tool rotates along an axis perpendicular to the workpiece, while the rotational axis of UPSM is parallel to the machined surface. Due to the unique machining principle of UPSM, the generation mechanism of the hybrid surfaces is introduced, and the optimal tool path generation strategy is detailed considering the compensation of the swing radius and tilting geometry of the diamond tool. Besides, the selecting criteria of the machining parameters is also discussed to ensure the ductile machining of brittle IR materials. In practical, two types of hybrid micro-optic components, namely hybrid micro-aspheric arrays and sinusoid grid surface with high-frequent secondary unidirectional phase gratings, were fabricated on a single-crystal silicon wafer. The acquired surface quality and the characteristics of the diffractive performances are further identified and analyzed in this study.

Optics EXPRESS

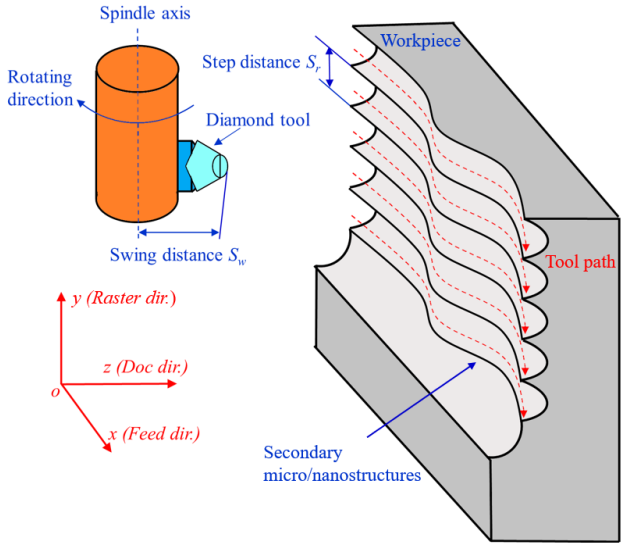

Fig. 1. Schematic of the machining approach for hybrid surfaces with secondary micro/nanostructures.

2. Principle for one-step generation of hybrid micro-optics

Hybrid micro-optics are characterized as high-frequent secondary micro/nanostructures superposed on a low-frequent primary surface with arbitrary shapes. In UPSM, the primary surface of the hybrid micro-optics is constructed via the removal of workpiece material, and the high-frequency secondary micro/nanostructures are simultaneously formed by the interference of the diamond tool edge between two neighboring raster cutting trajectories. The machining principle of UPSM for hybrid micro-optics is illustrated in Fig. 1. A diamond tool is fixed on the high-speed spindle with an adjustable swing radius. During the machining process, the rotating spindle horizontally feeds in the x direction, and the diamond tool intermittently cuts into and out of the workpiece surface with a specific depth of cut. In the meantime, the workpiece performs the transitional servo motions in z direction, just like slow tool servo, so as to deterministically generate the desired primary surface. After finishing one profile of cutting, a step motion along the raster direction (y direction) is carried out on the diamond tool, so the whole workpiece can be covered by material removal. In this way, secondary micro/nanostructures with desired shapes are flexibility generated using the tool residual marks through actively controlling the step interpolation in the raster direction.

The strategy of UPSM for hybrid micro-optics with desired primary surface and secondary micro/nanostructures is shown in Fig. 2. To avoid the interference of the cutting trajectories on the finished surface, the swing radius of the diamond tool should be selected first according to the smallest curvature radius of the desired primary surface. Then, the step interpolation of the raster movement is determined according to the desired shape of the secondary micro/nanostructures. It worth to note that micro/nanostructures with different cross-sectional profiles (including arc-shape, V-shape and rectangle) can be obtained by adopting the diamond tools with different edge shapes. By compensating the swing radius and the geometry tilt of the diamond tool, the toolpath is generated for the desired hybrid surfaces. To avoid brittle fracturs of IR materials, feed rates need to be carefully selected based on the ductile machining model for UPSM. Finally, the machined hybrid micro-optics are characterized by optical surface profiler to evaluate the surface quality and form error. The diffractive experiments are also conducted to evaluate the reflective diffraction characteristics of the generated hybrid surfaces.

Optics EXPRESS

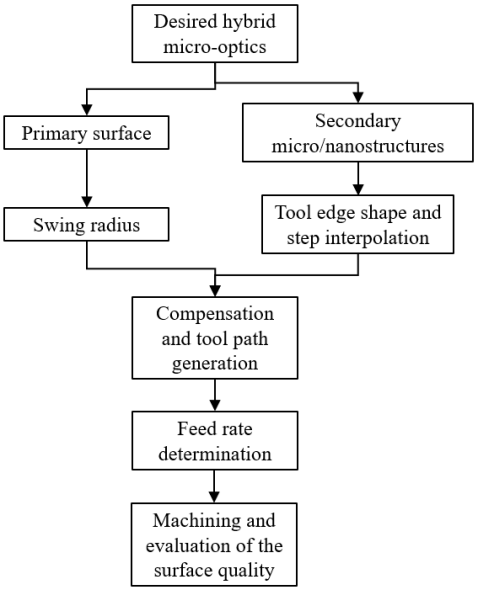

Fig. 2. Strategy of UPSM for hybrid micro-optics.

Due to the unique cutting process of UPSM, the following advantages for fabricating hybrid micro-optics on IR materials can be achieved: (i) the primary surface and the secondary micro/nanostructures of the desired micro-optics can be simultaneously generated, without needing complicated machining processes that combines several machining technologies; (ii) deep ductile machining depth on IR materials can be achieved by the intermittent material removal process of UPSM, which increases the achievable azimuthal height variation of IR optical components; (iii) high-frequent diffractive structures with different shapes are flexibly constructed, which is difficult to be achieved by fast and slow tool servo due to the restriction of the feeding bandwidth of the hardware servo system; (iv) the hybrid optical surfaces are generated in a deterministic way, so the form accuracy can be well guaranteed.

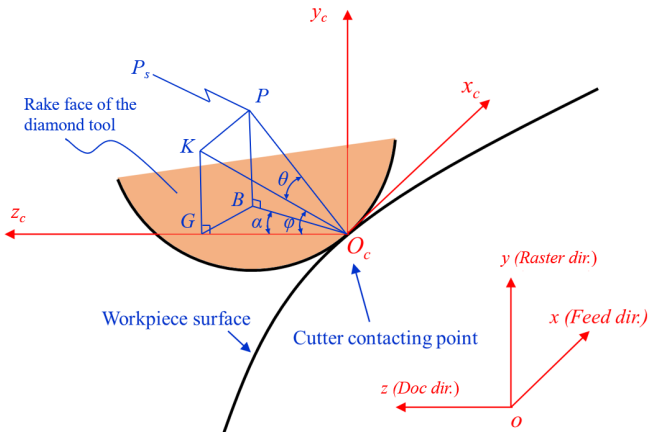

Fig. 3. Geometrical relation between the diamond tool and the workpiece surface.

3. Optimal toolpath generation for the UPSM

The unique machining principle of UPSM leads to a different toolpath determination strategy compared with conventional diamond milling. In UPSM, the swing center point (SCP) needs

Optics EXPRESS

to be determined as the toolpath according to the shapes of the desired hybrid optical surfaces. To determine the appropriate SCPs for the desired hybrid surfaces, the swing radius and the geometry tilt of the diamond tool should be compensated by the compensation algorithm. Then, the selecting criteria of the machining parameters are detailed to avoid the brittle fracturs of IR materials.

3.1 Compensation and determination of toolpath

In UPSM, the toolpath for the desired hybrid surface is decomposed into the 3-axis transitional servo motions of the milling machine, and hybrid surfaces are generated by the alternative feed and raster motions of the rotational diamond tool. Thus, the projected toolpath of UPSM is a set of parallel lines along feed direction with a constant length (L). Differential approach is adopted to determine the SCPs. The length of the feed motion is uniformly discretized into (N_s + 1) points. As shown in Fig. 3, a coordinate system (o_c-$x_cy_cz_c$) is built on the cutter contacting point with the x_c-axis and z_c-axis are parallel to the feed and raster direction, respectively. For the n-th point of the m-th feed motion cycle, the coordinate of the cutter contacting point $O_c^{(m,n)}$, denoted as $(x_c^{(m,n)}, y_c^{(m,n)}, z_c^{(m,n)})$, can be expressed by:

$$\begin{cases} x_c^{(m,n)} = \dfrac{n}{N_s} L \\ y_c^{(m,n)} = mS_r \\ z_c^{(m,n)} = F(x_c^{(m,n)}, y_c^{(m,n)}) \end{cases} \tag{1}$$

where S_r represents the step distance in the raster direction, and $F(x, y)$ is the expression of the desired primary surface of the hybrid micro-optics. Due to ever-changing topography of the hybrid surface, the rake face of the diamond tool will always be tilted with respect to the depth of cut direction (z_c-axis) and raster direction (y_c-axis) with the tilting angles $\theta^{(m,n)}$ and $\varphi^{(m,n)}$, respectively. As shown in Fig. 3, Point $P_t^{(m,n)}$ is the corresponding the tool nose center point for $O_c^{(m,n)}$, whose coordinate $(x_t^{(m,n)}, y_t^{(m,n)}, z_t^{(m,n)})$ is denoted as:

$$\begin{cases} x_t^{(m,n)} = x_c^{(m,n)} + R\sin\theta^{(m,n)} \\ y_t^{(m,n)} = y_c^{(m,n)} + R\cos\theta^{(m,n)}\sin\varphi^{(m,n)} \\ z_t^{(m,n)} = z_c^{(m,n)} + R\cos\theta^{(m,n)}\cos\varphi^{(m,n)} \end{cases} \tag{2}$$

where R is the tool nose radius. As shown in Fig. 3, line PK is perpendicular to line KO_c and line KG is perpendicular to line GO_c. Based on the geometry relation, the corresponding tiling angles $\alpha^{(m,n)}$, $\theta^{(m,n)}$ and $\varphi^{(m,n)}$ can be acquired as follows:

$$\begin{cases} \alpha^{(m,n)} = -\arctan\dfrac{\partial F(x_c^{(m,n)}, y_c^{(m,n)})}{\partial x_c^{(m,n)}} \\ \theta^{(m,n)} = \arctan\dfrac{\partial F(x_c^{(m,n)}, y_c^{(m,n)})}{\partial y_c^{(m,n)}} \\ \varphi^{(m,n)} = \arctan(\cos\theta^{(m,n)}\tan\alpha^{(m,n)}) \end{cases} \tag{3}$$

Different from fast and slow tool servo, the tool nose center points cannot be directly used as the tool path due to the rotation cutting trajectory for UPSM. In contrast, the coordinate of

Optics EXPRESS

SCPs, denoted as $(x_s^{(m,n)}, y_s^{(m,n)}, z_s^{(m,n)})$, is not determined by the rotational angle of the diamond tool, so SCPs are used as the toolpath for the hybrid surfaces. According to Eqs. (1) and (2), the coordinate of the SCP can be calculated as:

$$\begin{cases} x_s^{(m,n)} = x_c^{(m,n)} + R\sin\theta^{(m,n)} + (S_w - R)\sin\alpha^{(m,n)} \\ y_s^{(m,n)} = y_c^{(m,n)} + R\cos\theta^{(m,n)}\sin\varphi^{(m,n)} \\ z_s^{(m,n)} = z_c^{(m,n)} + R\cos\theta^{(m,n)}\cos\varphi^{(m,n)} + (S_w - R)\cos\alpha^{(m,n)} \end{cases} \tag{4}$$

where S_w is the swing radius of the diamond tool. Following the aforementioned steps, the SCPs can be well determined according to the desired primary surface of the hybrid micro-optics.

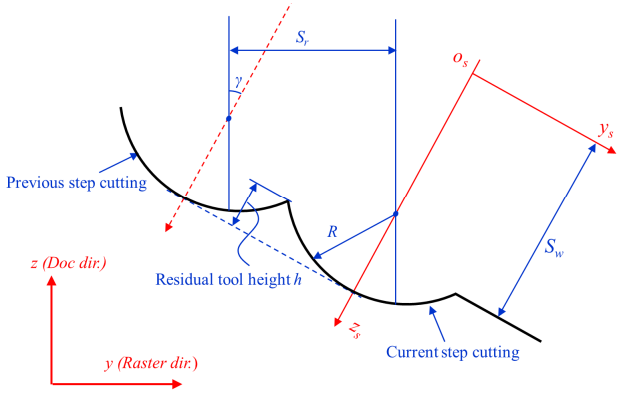

Fig. 4. Geometrical relation between the residual tool height and the step distance.

3.2 Machining parameters

According to the principle of UPSM, three machining parameters, namely swing radius, step distance in raster direction and feed rate, need to be determined before conducting the machining operation. To avoid the interference of the diamond tool, swing radius should be determined first based on the curvature radius of the desired primary surface. For convex primary surface, there is no limit on the swing radius, while for concave surface the swing radius should be less than the minimum curvature radius of the primary surface in feed direction, which is expressed as follows:

$$S_w < \min\left[\left|\frac{(1+(\frac{\partial F}{\partial x})^2)^{\frac{3}{2}}}{\frac{\partial^2 F}{\partial x^2}}\right|\right] \tag{5}$$

As learned from the surface generation principle of UPSM, the size of the secondary micro/nanostructures is not only determined by the step distance, but also influenced by the changing curvature of the primary surface. Nevertheless, in the previous toolpath generation strategies, the uniformity of the tool residual marks is generally neglected by employing evenly spaced step distance in the raster direction, which inevitably induces the non-uniform secondary diffractive structures in terms of size with the changing curvature of the primary surface [26]. Thus, an optimized algorithm with the consideration of the changing curvature is required to ensure the uniformity and the form accuracy of the secondary diffractive micro/nanostructures.

The geometrical relation between the height of the secondary micro/nanostructures and the step distance with the consideration of the changing curvature is shown in Fig. 4. To

Optics EXPRESS

obtain a constant height of the desired secondary micro/nanostructures (h), the step distance for the n-th point of the m-th feed motion cycle ($S_r^{(m,n)}$) is determined by the corresponding curvature. As the step distance is small in UPSM, the change of curvatures between two neighboring cutting points is regarded as unchanged in the algorithm. As shown in Fig. 4, an angle (γ) exists between the tangent line of the primary surface and the y-axis, the step distance in the raster direction can be calculated based on the geometric relation as:

$$S_r^{(m,n)} = 2\cos[\left|\arctan(\frac{\partial F}{\partial y})\right|]\times\sqrt{h(2R-h)} \tag{6}$$

where h is the height of the desired secondary structures, and R is the tool nose radius which determines the shape and width of the secondary structures. As a result, the height of secondary micro/nanostructures can be well controlled by adopting appropriated step distance calculated by Eq. (6).

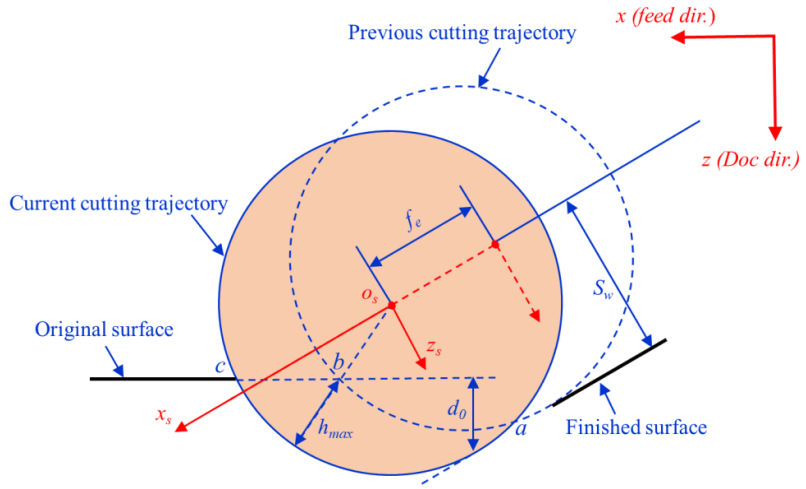

Fig. 5. Schematic of UPSM viewed along the y direction.

To avoid the brittle fractures and micro-cracks of IR materials in diamond cutting, the undeformed chip thickness needs to remain lower the critical depth of cut (DoC) of the IR material [27–29]. The chips of UPSM are intermittently formed as a result of two consecutive cutting processes, namely the current rotary cutting and the previous rotary cutting. In order to acquire a smooth surface, the maximum chip thickness (h_{max}) is required to be less than the critical DoC. As shown in Fig. 5, a tilting angle exits between the finished surface and the original surface in feed direction due to the curvature of the primary surface. As the space between two neighboring swing center points is very small in UPSM, the change of the curvature is neglected in the calculation, and the trochoidal cutting trajectory is equivalent to separate circles. The chip thickness of UPSM approaches zero at point a, then increases to the maximum chip thickness at point b. Based on the geometric relation, the coordinates of point b (x_b, z_b) in the o_s-$x_s z_s$ system can be calculated by the follow equations:

$$\begin{cases} x_b = -f_e + \sqrt{S_w^{\,2} - y_b^{\,2}} \\ y_b = \dfrac{\partial F}{\partial x}\times x_b + S_w - \dfrac{d_0}{\cos(\left|\arctan(\dfrac{\partial F}{\partial x})\right|)} \end{cases} \tag{7}$$

Optics EXPRESS

where f is the feed rate in μm/r and d_0 denotes the depth of cut. After determining the (x_b, z_b), the maximum chip thickness (h_{max}) can be obtained by:

$$h_{max} = S_w - \sqrt{(x_b^2 + y_b^2)} \tag{8}$$

Equations (7) and (8) are used to calculate the maximum chip thickness (h_{max}) of UPSM under a specific group of machining parameters, i.e., feed rate and depth of cut. If the calculated h_{max} is smaller than the critical DoC of silicon, ductile material removal process can be ensured. For a desired hybrid surfaces, the larger the height variation of its primary surface, the deeper depth of cut is required in the machining process. It is well known that the critical depth of cut is determined by the material characteristics [27–29]. As the critical depth of cut is generally calculated based on the empirical formula [21,30], the result is not quite accurate. To acquire the accurate critical DoC of silicon, experiment method is applied by sculpturing silicon for a taper groove with increasing cutting depth in this study. Figure 6 shows the cross-sectional profile of the taper groove in <100> direction. Obvious ductile-brittle transition can be observed with a depth of 148 nm, which is the critical DoC of the silicon wafer [31,32]. Thus, according to the critical DoC of silicon and the height variation of the primary surface, appropriate feed rates can be calculated from Eqs. (7) and (8) to ensure the ductile machining process of UPSM.

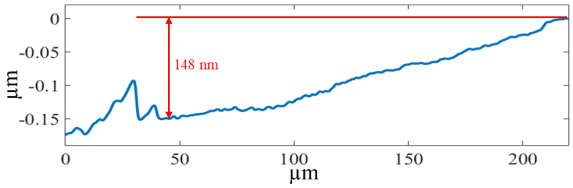

Fig. 6. Cross-sectional profile of the taper groove in <100> direction.

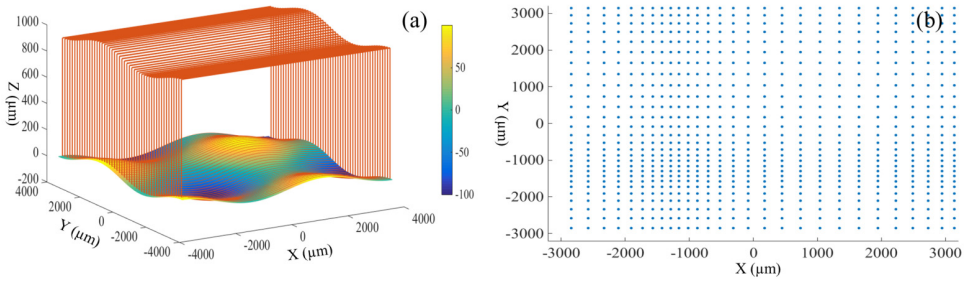

Fig. 7. Schematic of (a) the toolpath and (b) the SCPs in x-y plane.

Figure 7(a) shows the toolpath for a hybrid sinusoid surface with periodicity of 5 mm and amplitude of about 25 μm. A step distance of 20 μm is adopted in the raster direction. As shown in Fig. 7(a), the toolpath is smooth and characterized by a set of parallel lines in feed direction. Thus, this machining strategy offers an unchanged feed direction with respect to the crystallographic direction of the single-crystal IR materials, such as single-crystal silicon, which effectively avoid the undesired radial-spoke marks generated in fast and slow tool servo [18,33]. Besides, the SCPs is not uniformly distributed in the x-y plane, as shown in Fig. 7(b). This varying distance between two adjacent SCPs in both feed and raster directions is induced by the varying curvature radius of the primary surface, which indicates the effectiveness of the compensation algorithm of the swing radius and the tilt of the diamond tool. More importantly, this unique machining strategy of UPSM makes the generation of the secondary micro/nanostructures only dependent on the geometry and step distance of the diamond tool, instead of the dynamic property of the machining system. As a result, hybrid

Optics EXPRESS

micro-optics with high-frequent secondary micro/nanostructures can be deterministically generated with one step in a much easier way.

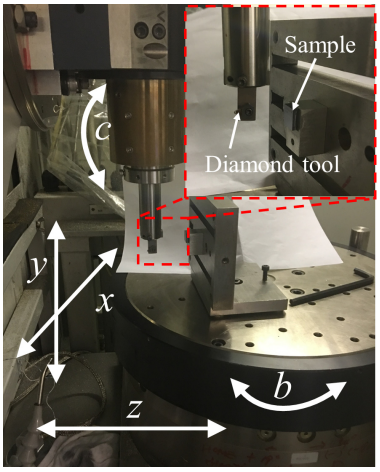

Fig. 8. Picture of the milling system.

4. Experimental setup

A five-axis milling machine (Precitech 705G) with two rotational tables and three translational servo slides was applied in UPSM of hybrid micro-optics on IR materials, as shown in Fig. 8. The workpiece glued on a fixture was installed on the parallel rotational table (*b*-axis). The tilting angle along feed direction can be minimized by carefully turning the rotation angle of the rotary table. After that the titling angle along raster direction is minimized by changing the pressing force on the back of the fixture. After the adjustment, the height variation along both feed and raster direction can be reduced to 1~2 μm with a sampling length of 10 mm. A commercial single-crystal diamond tool is clamped on the end of the spindle in *z*-axis with an adjustable swing radius. The workpiece material is single-crystal silicon, a typical IR material applied in infrared optics. The Young's elastic modulus is 160 Gpa, and the hardness is 12 Gpa. A three-dimensional non-contact optical measurement system provided by Zygo Corporation was then applied to capture the corresponding micro-topographies with proper magnification. To acquire a large measurement area, a set of small profiles were pitched together using the analysis software of the Zygo profiler.

To validate the proposed method, two types of hybrid micro-optic components, namely micro-aspheric arrays and sinusoid grid surface with high-frequent secondary unidirectional phase gratings, were fabricated on a single-crystal silicon wafer. The pitch and height of the desired nano-grooves is 24 μm and 620 nm, respectively. The shape of the secondary unidirectional phase gratings is the same with that of tool edge shape. The primary surface of each micro-aspheric arrays can be expressed by [34]:

$$z(x,y)=\frac{sCR_0^{\ 2}}{4+4\sqrt{1-(1+k)C^2R_0^{\ 2}}}-\frac{sC\rho^2(x,y)}{4+4\sqrt{1-(1+k)C^2\rho^2(x,y)}} \tag{9}$$

where s is the shape coefficient determining the concave-convex characteristic of the micro-aspheric surface; k determines the conic constant; C represents the curvature; R_0 is the radius of the micro-aspheric surface. Ordered nano-microgrooves were superimposed on the primary surface, which serve as the secondary unidirectional phase gratings, the expression of the primary surface of the sinusoid surface is

$$z(x,y)=A_x\sin(2\pi f_x x)+A_y\sin(2\pi f_y y) \tag{10}$$

Optics EXPRESS

where $A_x = A_y = 6$ μm and $f_x = f_y = 0.2 \times 10^{-3}$. Two diamond tools with different nose radius were applied for the hybrid micro-aspheric arrays and hybrid sinusoid grid surface, respectively (see Table 1). The adopted diamond tools have a rake angle of −25°, while the clearance angle is 10°. The machining parameters are detailed in Table 2.

Table 1. Structure parameters used for the primary micro-aspheric surface.

Shape coefficient s	−1
Radius of the array R_0	0.223 mm
Conic constant k	−0.8
Curvature C	0.2 mm^{-1}

Table 2. Machining parameters used for the hybrid micro-aspheric and sinusoid surfaces.

Machining parameters	Hybrid micro-aspheric surface	Hybrid sinusoid surface
Swing radius (mm)	5	15.5
Spindle rotation rate (rpm)	7000	4000
Step distance (μm)	24	40
Tool nose radius (mm)	0.12	0.27
Material	Single-crystal silicon	Single-crystal silicon
Cutting direction	<100>	<100>
Depth of cut (μm)	3	5
Feed rate (μm/r)	2	4

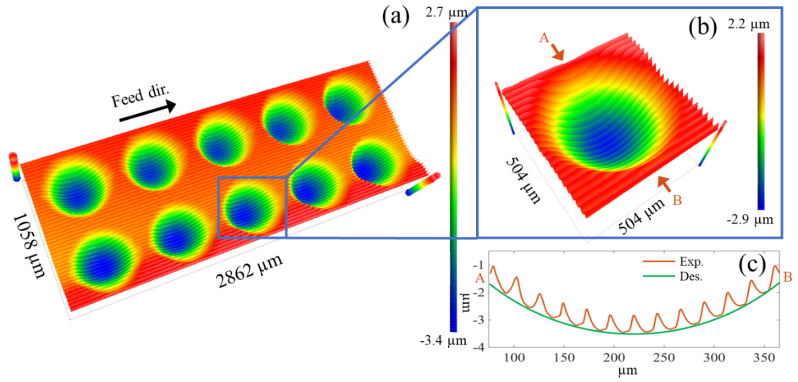

Fig. 9. Characteristics of the machined hybrid micro-aspheric arrays, (a) a large area view, (b) for an individual structure and (c) cross-sectional profile.

5. Results and discussion

To validate the feasibility of the proposed UPSM, two types of hybrid micro-optics including hybrid micro-aspheric arrays and hybrid sinusoid grid surface with high-frequent unidirectional phase gratings, were fabricated on a single-crystal silicon wafer. The characteristics of the generated hybrid surfaces are discussed in this section, and the corresponding reflective diffraction characteristic is also analyzed.

5.1 Micro-aspheric arrays with nano-gratings

Figure 9 illustrates the characteristics of the generated hybrid micro-aspheric arrays. An overview of the hierarchical surface topographies is shown in Fig. 9(a), which is captured by the stitched optical images with a 5 times amplification. It can be observed that a total of 10

Optics EXPRESS

hybrid micro-aspheric lens with secondary parallel nano-grooves are uniformly distributed in two lines. Figure 9(b) further shows an enlarged view of a hybrid micro-aspheric profile, which is captured by a 20 times amplification. As the secondary nano-grooves are formed by the periodic raster movement of the diamond tool, these nano-grooves are unidirectionally distributed with respect to raster direction. As shown in Fig. 9(c), the characteristics of the hybrid micro-aspheric structure can be more clearly observed by the cross-sectional profile in raster direction. It is observed that the cross-sectional profile is characterized as a curved primary surface imposed by a set of high-frequent arc-shaped nanostructures.

As shown in Figs. 10(b) and 10(c), through directly subtracting the secondary nano-grooves, the hierarchical surface is further divided into the primary aspheric surface and a nanostructured surface. Moreover, the shapes of the secondary nano-grooves are perfectly in accordance with the edges of the diamond tool, as shown in Fig. 10(d). The mean value of the pitch and the height of the nano-grooves is 24.1 μm and 607.5 nm, respectively. In view of the curvature change of the primary surface, the pitch and height of the desired nano-grooves is 24 μm and 620 nm, respectively. Thus, the generated height and pitch commonly present a good agreement with that of desired nano-grooves, with a slight deviation of 2%. This deviation can be regarded as the form error of the generated hybrid micro-aspheric surfaces, which might jointly result from the material spring back and kinematic error of the machine tool. Besides, the green envelop curve of the secondary nanogrooves that is shown in Fig. 9(c) is in good accordance with the desired primary surface derive from Eq. (9), which strongly validates the feasibility of the UPSM for deterministic generation of IR hybrid micro-optics with high form accuracy.

To fulfill the optical application, the maximum allowable form error of an optical element is λ/4 of the transmitted light [35]. As single-crystal silicon is normally used in IR optical area that transmits the light with wavelength ranging from 1.2 μm to 6 μm. As a result, the required form error for a silicon micro-groove needs to be less than 300 nm PV for a 1.2 μm wavelength, in order to avoid the distortion of the gathered profile. The experiment results validate that the height and pitch of the generated secondary diffractive nanostructures present a good agreement with that of desired ones, with a form error about 0.1 μm, which fulfils the requirement of IR application.

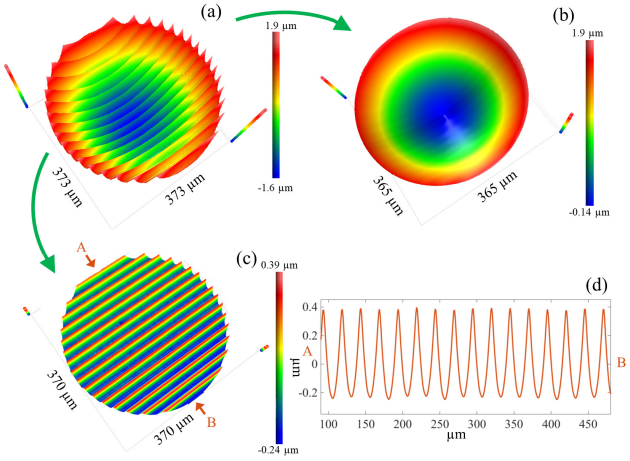

Fig. 10. 3D topographies of (a) generated hierarchical micro-aspheric surface, (b) the filter primary aspheric surface, (c) the extracted secondary nano-grooves and (d) 2D profile in cross-sectional direction after removing the primary profile.

Optics EXPRESS

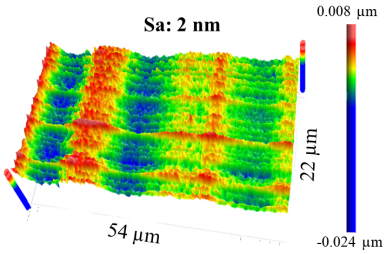

Fig. 11. Micro-topography of the generated surface.

Through removing the groove shape from the hybrid micro-aspheric structure in a small area, the corresponding micro-topography can be acquired, as shown in Fig. 11. Very small surface roughness value was obtained at Sa = 2 nm, indicating the ductile material removal without brittle fractures. More importantly, both the acquired 3D surface topographies and the 2D cross-sectional profiles are very smooth, as shown in Fig. 10, which further validate capability of UPSM in ductile machining of IR materials for desired hybrid micro-optics. Obviously, the micro-topography of the micro-grooves is characterized as undesired stripe patterns that is vertical to the feed direction, which should correspond to the tool residual marks. These marks may be caused by the intermittent cutting operation of UPSM. To obscure these marks, large swing radius and small feed rates are possibly adopted.

Generally, researcher use an index named total integrated scattering (*TIS*) to evaluate the optimal performance of an optical component [18,36]. According to Harvey et al. [36], TIS smaller than 0.01 is acceptable for most optical systems, and TIS can be expressed by

$$TIS \approx (\frac{4\pi\delta}{\lambda})^2 \tag{11}$$

where λ is the incident light wavelength and δ denotes the RMS surface roughness Rq. As single-crystal silicon is normally used to transmit the infrared light with wavelength ranging from 1.2 µm to 6 µm, the surface roughness is required to be less than 10 nm Rq. To simplify the calculation, the required Ra is estimated as 0.8 that of Rq, so surface roughness lower than 8 nm Ra is required for the IR optical components made by single-crystal silicon. The surface roughness acquired in the study is 2 nm Sa fulfils the requirement. In the revised manuscript, the assessment of the finished surface quality from the view of optical performance is added and highlighted.

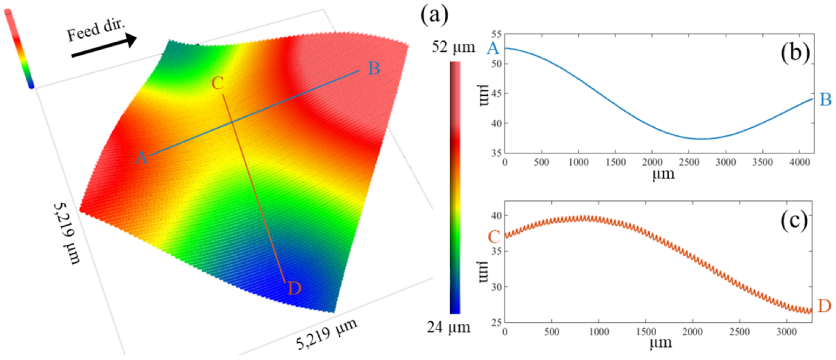

Fig. 12. (a) 3D topography of the generated hybrid sinusoid freeform surface and its cross-sectional profiles in (b) feed direction and (c) raster direction.

5.2 Sinusoid freeform surface with nano-gratings

To further validate the effectiveness of UPSM, another kind of hybrid micro-optics with much large height variation, namely hybrid sinusoid surface with secondary diffractive phase

Optics EXPRESS

gratings, is also deigned and machined. The mathematical expression of the primary sinusoid freeform surface is described by Eq. (10). Figure 12(a) illustrates the 3D topography of the generated hybrid sinusoid freeform surface, whose largest height variation is about 25 μm. It is known that due to the hard-and-brittle nature of silicon, it is difficult to fabricate freeform silicon optical components with large height variation, while guaranteeing ultra-smooth surface quality by fast and slow tool servo. As shown in Fig. 13, the microscope image of the generated surface by UPSM is very smooth without brittle fractures. This is majorly attributed to the intermittent cutting process UPSM, in which way very small chip thickness can be generated even under large depth of cut. Thus, UPSM is more superior to generate IR optics with large variation for a variety of shapes.

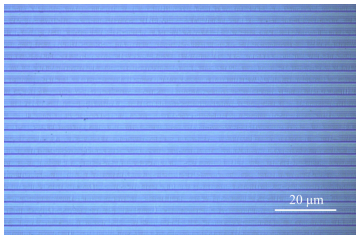

Fig. 13. Microscope image of the generated sinusoid freeform surface in a small zone.

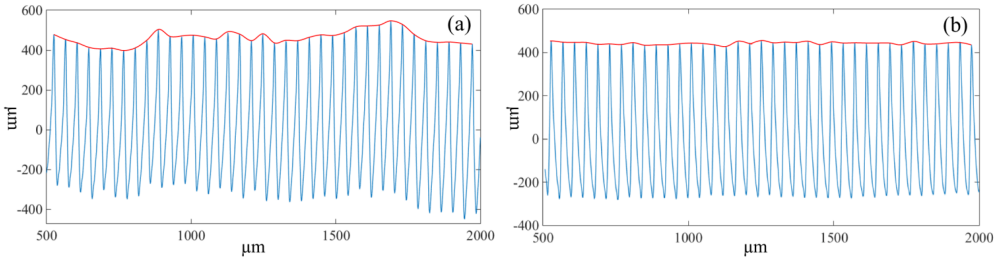

Fig. 14. 2D profiles in cross-sectional direction after removing the primary profile by (a) ordinary algorithm and (b) optimized algorithm.

Figures 14(a) and 14(b) compare the 2D profiles of the hybrid sinusoid freeform surface generated by ordinary algorithm and the optimized algorithm, respectively. It is obvious that the secondary nanostructures generated by ordinary algorithm is more non-uniform in height, and a very bumpier envelope line is observed on the top of the secondary nanostructures. This is caused by the change of the curvature in the raster direction. In comparison, the envelop line of the secondary nanostructures generated by the optimized algorithm is much smoother, which is attributed to the consideration of the changing curvature in the calculation of step distance as expressed in Eq. (6).

The major advantage of the proposed UPSM in fabricating hybrid infrared optics is that the primary reflective/refractive surface and the secondary diffractive nanostructures of the hybrid micro-optics can be simultaneously generated, without complicated machining processes. In comparison, for previous methods, multi-step processes that combines ultra-precision machining technologies and non-mechanical methods were normally required to obtain the hybrid IR micro-optics with desired shapes [6,8]. However, this multi-step processes not only introduce unnecessary machining errors, but also is relatively high-cost and low-efficient. More importantly, the form accuracy acquired by etching processes is generally difficult to control. In contrast, it is learned from the experiment results from Fig. 8 and Fig. 12, very high form accuracy and smooth finished surface quality are achieved, which is also validate the superiority of UPSM.

Besides, high-frequent diffractive structures with different shapes are flexibly constructed by UPSM, which is difficult to be achieved by fast and slow tool servo (FTS/STS) due to the

Optics EXPRESS

restriction of the feeding bandwidth of the hardware servo system. It is known that the periodicity of the secondary structures generated by FTS/STS is in an order of several hundred micrometers [37]. In contrast, the periodicity of the secondary diffractive nanostructures generated by UPSM is about 20 μm, as shown in Fig. 9, which is much less than that of FTS/STS. Especially, as learned from the machining principle of UPSM, an even smaller periodicity can be easily achieved by UPSM regardless of the moving bandwidth limitation of the servo system, as the secondary diffractive micro/nanostructures are constructed by the interference of two neighboring raster cutting operations in UPSM, which is the advantage of UPSM.

Moreover, the unidirectional characteristics of the secondary nano-gratings can be clearly illustrated in Figs. 11(b) and 11(c). Smooth profile without nano-gratings can be observed on the cross-sectional profile in feed direction, while sinusoid profile with imposition of secondary arc-shaped micro/nanogrooves is acquired in the raster direction. This unidirectional property leads to a unique reflective diffraction characteristic. As illustrated in Fig. 15, a set of even-distributed light spots can be acquired from the diffractive light obtained from the hybrid sinusoid freeform surface. In contrast, only a diffractive spot is observed from the diffractive light of the conventional sinusoid surface. This unique optical property may be useful in the optics design for special infrared imaging system and light path correction [38,39]. Further, this hierarchical surface can be designed to be an integrated hybrid IR optical component with both reflective/refractive primary surface and high-frequent secondary diffractive nanostructures [8].

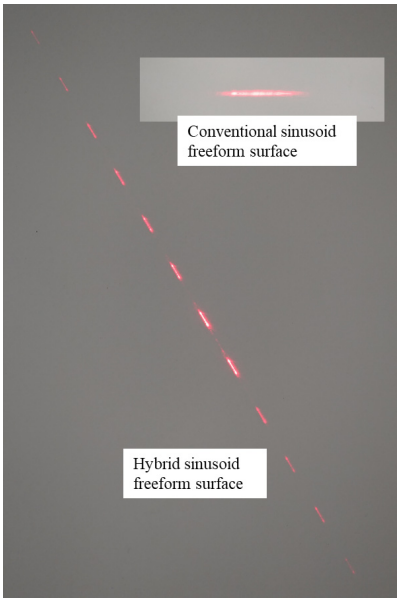

Fig. 15. Reflective diffraction characteristics of the hybrid sinusoid freeform surface.

6. Conclusions

In the present study, a novel ultra-precision side milling (UPSM) method has been adopted and demonstrated to achieve one-step generation of hybrid micro-optics on infrared (IR) materials with high form accuracy. This approach effectively overcomes the difficulties in fabricating complicated hierarchical structures on hard-and-brittle IR materials with very low defects. Further, based on this machining strategy, both the primary refractive/reflective freeform surface and secondary diffractive nanostructures are formed within one-step operation, which accordingly is more beneficial to reduce the processing time and improve the machining accuracy. The main conclusions can be summarized as follows:

Optics EXPRESS

(1) In UPSM, the primary surface of the hybrid micro-optics is formed by the removal of workpiece material, and the high-frequency secondary micro/nanostructures are simultaneously formed by the interference of the diamond tool edge between two neighboring raster cutting operations. Thus, very high-frequent diffractive secondary structures can be conveniently construed by adjusting the step distance in raster direction, without the limitation of the bandwidth of the hardware servo system.

(2) Via the intermittent material removal process of UPSM, very small chip thickness can be realized even under a large depth of cut, which is beneficial to ductile machining of brittle IR materials. This approach provides a guidance to simultaneously fabricate complicated hierarchical structures on brittle IR materials with ultra-precision form accuracy and ultra-smooth surface quality.

(3) Two types of hybrid micro-optic components, namely micro-aspheric arrays and sinusoid grid surface with high-frequent secondary unidirectional phase gratings, are successfully fabricated on single-crystal silicon to validate the proposed method. The generated surfaces present a good agreement with that of desired ones, with a slight deviation of 2%. Smooth surface with a roughness of 2 nm Sa is achieved.

(4) The unidirectional diffractive nanostructures of the generated hybrid micro-optics lead to a set of even-distributed diffractive light spots, while the diffractive light from the conventional sinusoid surface only include a diffractive spot. This unique optical property provides more imaginations in the design of IR optical systems.

Funding

Research Committee of the Hong Kong Polytechnic University (Project Code: RUNS); National Natural Science Foundation of China (51675455)

Acknowledgments

This work was supported partially by the Research Committee of The Hong Kong Polytechnic University (Project Code: RUNS) and the National Natural Science Foundation of China (51675455).

References

1. S. Liu, J. A. Mulligan, and S. G. Adie, "Volumetric optical coherence microscopy with a high space-bandwidth-*time* product enabled by hybrid adaptive optics," Biomed. Opt. Express **9**(7), 3137–3152 (2018).
2. Y. Pang, Y. Li, M. Yan, D. Liu, J. Wang, Z. Xu, and S. Qu, "Hybrid metasurfaces for microwave reflection and infrared emission reduction," Opt. Express **26**(9), 11950–11958 (2018).
3. M. Malinauskas, A. Žukauskas, V. Purlys, K. Belazaras, A. Momot, D. Paipulas, R. Gadonas, A. Piskarskas, H. Gilbergs, A. Gaidukevičiūtė, I. Sakellari, M. Farsari, and S. Juodkazis, "Femtosecond laser polymerization of hybrid/integrated micro-optical elements and their characterization," J. Opt. **12**(12), 124010 (2010).
4. D.-H. Ko, J. R. Tumbleston, K. J. Henderson, L. E. Euliss, J. M. DeSimone, R. Lopez, and E. T. Samulski, "Biomimetic microlens array with antireflective "moth-eye" surface," Soft Matter **7**(14), 6404–6407 (2011).
5. Z. Sun, S. To, and S. Zhang, "A novel ductile machining model of single-crystal silicon for freeform surfaces with large azimuthal height variation by ultra-precision fly cutting," Int. J. Mach. Tools Manuf. **135**, 1–11 (2018).
6. Z. Deng, Q. Yang, F. Chen, X. Meng, H. Bian, J. Yong, C. Shan, and X. Hou, "Fabrication of large-area concave microlens array on silicon by femtosecond laser micromachining," Opt. Lett. **40**(9), 1928–1931 (2015).
7. H. Zhang, L. Li, S. Scheiding, A. Gebhardt, S. Risse, R. Eberhardt, A. Tünnermann, D. Yao, and Y. Y. Allen, "Fabrication of three-dimensional functional microstructures on curved substrates using three-dimensional microlens projection," J. Micro Nano-Manuf. **1**(3), 031006 (2013).
8. R. Kleindienst, R. Kampmann, S. Stoebenau, and S. Sinzinger, "Hybrid optical (freeform) components--functionalization of nonplanar optical surfaces by direct picosecond laser ablation," Appl. Opt. **50**(19), 3221–3228 (2011).
9. J. Kim, N. Takama, B. Kim, and H. Fujita, "Optical-softlithographic technology for patterning on curved surfaces," J. Micromech. Microeng. **19**(5), 055017 (2009).
10. Y. Chen, "Nanofabrication by electron beam lithography and its applications: a review," Microelectron. Eng. **135**, 57–72 (2015).

Optics EXPRESS

11. C. M. Waits, A. Modafe, and R. Ghodssi, "Investigation of gray-scale technology for large area 3D silicon MEMS structures," J. Micromech. Microeng. **13**(2), 170–177 (2002).
12. J. M. Ramirez, V. Vakarin, J. Frigerio, P. Chaisakul, D. Chrastina, X. Le Roux, A. Ballabio, L. Vivien, G. Isella, and D. Marris-Morini, "Ge-rich graded-index Si 1-xGex waveguides with broadband tight mode confinement and flat anomalous dispersion for nonlinear mid-infrared photonics," Opt. Express **25**(6), 6561–6567 (2017).
13. V. J. Kitsmiller, M. M. Dummer, K. Johnson, G. D. Cole, and T. D. O'Sullivan, "Frequency domain diffuse optical spectroscopy with a near-infrared tunable vertical cavity surface emitting laser," Opt. Express **26**(16), 21033–21043 (2018).
14. H. Zuo, D.-Y. Choi, X. Gai, B. Luther-Davies, and B. Zhang, "CMOS compatible fabrication of micro, nano convex silicon lens arrays by conformal chemical vapor deposition," Opt. Express **25**(4), 3069–3076 (2017).
15. Z. Li, F. Fang, J. Chen, and X. Zhang, "Machining approach of freeform optics on infrared materials via ultra-precision turning," Opt. Express **25**(3), 2051–2062 (2017).
16. B. S. Dutterer, J. L. Lineberger, P. J. Smilie, D. S. Hildebrand, T. A. Harriman, M. A. Davies, T. J. Suleski, and D. A. Lucca, "Diamond milling of an Alvarez lens in germanium," Precis. Eng. **38**(2), 398–408 (2014).
17. J. Zhang, N. Suzuki, Y. Wang, and E. Shamoto, "Fundamental investigation of ultra-precision ductile machining of tungsten carbide by applying elliptical vibration cutting with single crystal diamond," J. Mater. Process. Technol. **214**(11), 2644–2659 (2014).
18. M. Mukaida and J. Yan, "Ductile machining of single-crystal silicon for microlens arrays by ultraprecision diamond turning using a slow tool servo," Int. J. Mach. Tools Manuf. **115**, 2–14 (2017).
19. A. R. A. Manaf, T. Sugiyama, and J. Yan, "Design and fabrication of Si-HDPE hybrid Fresnel lenses for infrared imaging systems," Opt. Express **25**(2), 1202–1220 (2017).
20. Z. Li, F. Fang, X. Zhang, X. Liu, and H. Gao, "Highly efficient machining of non-circular freeform optics using fast tool servo assisted ultra-precision turning," Opt. Express **25**(21), 25243–25256 (2017).
21. S. Goel, X. Luo, A. Agrawal, and R. L. Reuben, "Diamond machining of silicon: a review of advances in molecular dynamics simulation," Int. J. Mach. Tools Manuf. **88**, 131–164 (2015).
22. J. Zhang, J. Zhang, T. Cui, Z. Hao, and A. Al Zahrani, "Sculpturing of single crystal silicon microstructures by elliptical vibration cutting," J. Manuf. Process. **29**, 389–398 (2017).
23. J. Zhang, T. Cui, C. Ge, Y. Sui, and H. Yang, "Review of micro/nano machining by utilizing elliptical vibration cutting," Int. J. Mach. Tools Manuf. **106**, 109–126 (2016).
24. S. Zhang, S. To, Z. Zhu, and G. Zhang, "A review of fly cutting applied to surface generation in ultra-precision machining," Int. J. Mach. Tools Manuf. **103**, 13–27 (2016).
25. F. Fang, X. Zhang, A. Weckenmann, G. Zhang, and C. Evans, "Manufacturing and measurement of freeform optics," CIRP Ann. **62**(2), 823–846 (2013).
26. L. Kong, "Modeling of ultra-precision raster milling and characterization of optical freeform surfaces," (Department of Industrial and Systems Engineering, The Hong Kong Polytechnic University, 2010).
27. T. G. Bifano, T. A. Dow, and R. O. Scattergood, "Ductile-regime grinding: a new technology for machining brittle materials," J. Eng. Ind. **113**(2), 184–189 (1991).
28. A. V. Gopal and P. V. Rao, "A new chip-thickness model for performance assessment of silicon carbide grinding," Int. J. Adv. Manuf. Technol. **24**(11-12), 816–820 (2004).
29. Z. Dong and H. Cheng, "Ductile mode grinding of reaction-bonded silicon carbide mirrors," Appl. Opt. **56**(26), 7404–7412 (2017).
30. S. Goel, X. Luo, P. Comley, R. L. Reuben, and A. Cox, "Brittle–ductile transition during diamond turning of single crystal silicon carbide," Int. J. Mach. Tools Manuf. **65**, 15–21 (2013).
31. G. Xiao, S. To, and E. Jelenković, "Effects of non-amorphizing hydrogen ion implantation on anisotropy in micro cutting of silicon," J. Mater. Process. Technol. **225**, 439–450 (2015).
32. J. Yan, T. Asami, H. Harada, and T. Kuriyagawa, "Fundamental investigation of subsurface damage in single crystalline silicon caused by diamond machining," Precis. Eng. **33**(4), 378–386 (2009).
33. M. Wang, W. Wang, and Z. Lu, "Anisotropy of machined surfaces involved in the ultra-precision turning of single-crystal silicon—a simulation and experimental study," Int. J. Adv. Manuf. Technol. **60**(5-8), 473–485 (2012).
34. D. Yu, Y. Wong, and G. Hong, "Ultraprecision machining of micro-structured functional surfaces on brittle materials," J. Micromech. Microeng. **21**(9), 095011 (2011).
35. H. Ottevaere, R. Cox, H.-P. Herzig, T. Miyashita, K. Naessens, M. Taghizadeh, R. Völkel, H. Woo, and H. Thienpont, "Comparing glass and plastic refractive microlenses fabricated with different technologies," J. Opt. A, Pure Appl. Opt. **8**(7), S407–S429 (2006).
36. J. E. Harvey, N. Choi, S. Schroeder, and A. Duparré, "Total integrated scatter from surfaces with arbitrary roughness, correlation widths, and incident angles," Opt. Eng. **51**(1), 013402 (2012).
37. L. Zhu, Z. Li, F. Fang, S. Huang, and X. Zhang, "Review on fast tool servo machining of optical freeform surfaces," Int. J. Adv. Manuf. Technol. **95**(5-8), 2071–2092 (2018).
38. D. Fattal, Z. Peng, T. Tran, S. Vo, M. Fiorentino, J. Brug, and R. G. Beausoleil, "A multi-directional backlight for a wide-angle, glasses-free three-dimensional display," Nature **495**(7441), 348–351 (2013).
39. T. Ando, T. Korenaga, M. A. Suzuki, and J. Tanida, "Diffraction light analysis method for a diffraction grating imaging lens," Appl. Opt. **53**(11), 2532–2538 (2014).